AFRL-AFOSR-JP-TR-2024-0007

Identification of anti-ferromagnetically coupled skyrmion pairs for quasi zero power computing: emulation of biological neuron/synapse functions

JIN PYO HONG
INDUSTRY UNIVERSITY COOPERATION FOUNDATION.HANYANG UNIVERSITY
222 WANGSIMNI-RO, SEONGDONG-GU
SEOUL, SEOUL, 04763
KOR

11/17/2023
Final Technical Report

Air Force Research Laboratory
Air Force Office of Scientific Research
Asian Office of Aerospace Research and Development
Unit 45002, APO AP 96338-5002

REPORT DOCUMENTATION PAGE

PLEASE DO NOT RETURN YOUR FORM TO THE ABOVE ORGANIZATION.

1. REPORT DATE	2. REPORT TYPE	3. DATES COVERED	
20231117	Final	START DATE 20211015	END DATE 20231014

4. TITLE AND SUBTITLE
Identification of anti-ferromagnetically coupled skyrmion pairs for quasi zero power computing: emulation of biological neuron/synapse functions

5a. CONTRACT NUMBER	5b. GRANT NUMBER	5c. PROGRAM ELEMENT NUMBER
	FA2386-22-1-0127	61102F

5d. PROJECT NUMBER	5e. TASK NUMBER	5f. WORK UNIT NUMBER

6. AUTHOR(S)
Jin Pyo Hong

7. PERFORMING ORGANIZATION NAME(S) AND ADDRESS(ES)
INDUSTRY UNIVERSITY COOPERATION FOUNDATION.HANYANG UNIVERSITY
222 WANGSIMNI-RO, SEONGDONG-GU
SEOUL, SEOUL 04763
KOR

8. PERFORMING ORGANIZATION REPORT NUMBER

9. SPONSORING/MONITORING AGENCY NAME(S) AND ADDRESS(ES)	10. SPONSOR/MONITOR'S ACRONYM(S)	11. SPONSOR/MONITOR'S REPORT NUMBER(S)
AOARD UNIT 45002 APO AP 96338-5002	AFRL/AFOSR IOA	AFRL-AFOSR-JP-TR-2024-0007

12. DISTRIBUTION/AVAILABILITY STATEMENT
A Distribution Unlimited: PB Public Release

13. SUPPLEMENTARY NOTES

14. ABSTRACT
Two main goals for our research were achieved 1) to grow the RKKY-coupled magnetic multilayers and efficient generation of AFC-SkP by employing multiple rf sputtering systems and their physical parameters, such as Dzyaloshinskii-Moriya interaction (DMI) and perpendicular magnetic anisotropy (PMA) energy contributions for the generation of magnetic skyrmion and 2) to exploit the fully coupled motion dynamics of antiferromagnetically coupled skrymion pairs (AFC-SkP) by building an anti-ferromagnetic coupled triple multilayer frames for emulation of AFC-SkP-driven basic neuron synapsis and neuron functions.

15. SUBJECT TERMS

16. SECURITY CLASSIFICATION OF:			17. LIMITATION OF ABSTRACT	18. NUMBER OF PAGES
a. REPORT	b. ABSTRACT	c. THIS PAGE		
U	U	U	SAR	30

19a. NAME OF RESPONSIBLE PERSON	19b. PHONE NUMBER *(Include area code)*
AKIRA NAMATAME	3152277010

Standard Form 298 (Rev.5/2020)
Prescribed by ANSI Std. Z39.18

[Final Report]

Asian Office of Aerospace Research and Development (AOARD)

Identification of anti-ferromagnetically coupled skyrmion pairs for quasi zero power computing: emulation of biological neuron/synapse functions

I. HEADING

A. Principal Investigator & Key Researcher

Name	Affiliation	Position
	Department	Field of Study/Final Degree
Jin Pyo Hong	Hanyang University	Professor (Dean, Collage of Natural Science)
	Physics	Ph. D

B. BAA Name:

FA9550-19-S-0003/or FA9550-18-S-003

Asian Office of Aerospace Research and Development (AOARD)

C. Most relevant BAA Section:

US-Korea Quantum Initiative

D. Proposal Title:

Identification of anti-ferromagnetically coupled skyrmion pairs for quasi zero power computing: emulation of biological neuron/synapse functions

E. Principle Investigator:

The PI (Jin Pyo Hong) has expertise in various spin dynamics and their device applications, including STT-MRAM, domain wall motion-based AI, and physics of a single skyrmion. In addition,

PI has been working on ion dynamics for the development of 3D stacked crossbar-array resistive random access memory, selectors, and their AI applications and has published the more than 150 papers since 1998.

F. Key Researcher(s) involved in the Proposed Project

Jin Pyo Hong: Department of Physics, Hanyang University (HYU), Seoul 04763, Republic of Korea
Jeong hun Shin: Department of Physics, Hanyang University (HYU), Seoul 04763, Republic of Korea
Jeon Woo Seo: Department of Physics, Hanyang University (HYU), Seoul 04763, Republic of Korea
Da Seul Hyeon, Department of Physics, Hanyang University (HYU), Seoul 04763, Republic of Korea

G. Proposed Period-of-Performance

15 Oct 2021 – 14 Oct 2023

H. Proposed Total Cost (for each year)

The requested budget is $ 44,000 per year for two years of proposed period of performance. The total $88,000 budget will cover graduate students' stipends, materials & supplies, travels, and indirect cost to complete the proposed project.

II. SCIENTIFIC AND TECHNICAL OBJECTIVES

A. Major Goals

Two main goals for our research are 1) to grow the RKKY-coupled magnetic multilayers and efficient generation of AFC-SkP by employing multiple rf sputtering systems and their physical parameters, such as Dzyaloshinskii-Moriya interaction (DMI) and perpendicular magnetic anisotropy (PMA) energy contributions for the generation of magnetic skyrmion and to exploit the fully coupled motion dynamics of antiferromagnetically coupled skrymion pairs (AFC-SkP) by building an anti-ferromagnetic coupled triple multilayer frames for emulation of AFC-SkP-driven basic neuron synapsis and neuron functions.

B. Experimental

1) Device fabrication

To provide antiferromagnetically coupled spins or dynamics in magnetic multi-layer configuration, at first, we fabricated a sandwiched synthetic antiferromagnetic (S-SyAF) system including a CoFeB (FM)/W (HM)/CoFeB (FM) stack as a crucial geometry by employing several rf/dc sputtering systems. A choice of suitable thickness of middle W layer was supposed to generate opposite spin currents (up and down) directed toward the top and bottom FM layers upon the application of electric current, in addition to enabling the Ruderman–Kittel–Kasuya–Yosida (RKKY) interaction: that is, the S-SyAF frame coupled with the RKKY interaction was expected to support the possibility of the generation of two opposite spins owing to the spin hall effect (SHE) in the middle HM layer. The S-SyAF stacks of MgO (1 nm)/CoFeB (1.3 nm)/W (2 nm)/CoFeB (1.3 nm)/MgO (1 nm)/Ta (3 nm) on a SiO_2 substrate were in-situ prepared without breaking the chamber. All layers were deposited by magnetron sputtering at a base pressure of 7×10^{-9} Torr, followed by post-annealing at 350 °C for 30 min under a perpendicular magnetic field of 3 T. After that, the S-SyAF frame were patterned by photo lithography and etched by ion milling techniques, together with the process of the Pt electrode contact.

2) Magnetic and electrical analyses

We systematically studied the magnetic characteristics containing more detailed individual M-H loops by utilizing a vibrating sample magnetometer, together with diverse structural investigation by scanning transmission electron microscopy (STEM) and XRD measurements. In addition, we conducted electrical analyses by choosing different device configurations for the identification of magnetic domain wall and skyrmion motions under electrical stimulus.

III. SUMMARIZED ACCOMPLISHMENTS for 1st YEAR

As an initial approach to identifying the possibility of domain wall motion (DWM)-based synapses and neuron functions, we had to consider the governing equation of DWM as follows:

$$H = -\vec{\mu} \cdot \vec{B} - J\vec{S}_1 \cdot \vec{S}_2 - \vec{D} \cdot (\vec{S}_1 \times \vec{S}_2) + K \sin^2\theta + Dipole\ energy, \text{-------- (1)}$$

where each term is a zeeman, exchange, DMI, PMA and dipole-dipole interaction energy contributions to the above Hamiltonian. To validate the experimental DWMs, we prepared the sample stacks of Si/SiO_2/1 nm MgO/1.2 nm $Co_{20}Fe_{60}B_{20}$/1.2 nm W/3 nm Ta with perpendicular magnetic anisotropy and then patterned by a Hall bar geometry. Fig.1 shows the representative external electrical pulse-driven DWMs (left) and their corresponding highly linear and symmetric variation in the hall resistance (R_H) as a function of the electrical pulse numbers during potentiation–depression operation (right). The results ensured the highly uniform drift of DWM under the consecutive identical positive and negative electrical pulses, thus reflecting the possibility of practical implementation in spin-synapsis weight behaviours when precise weight performance is attained by means of adjusting operation parameters and device configuration.

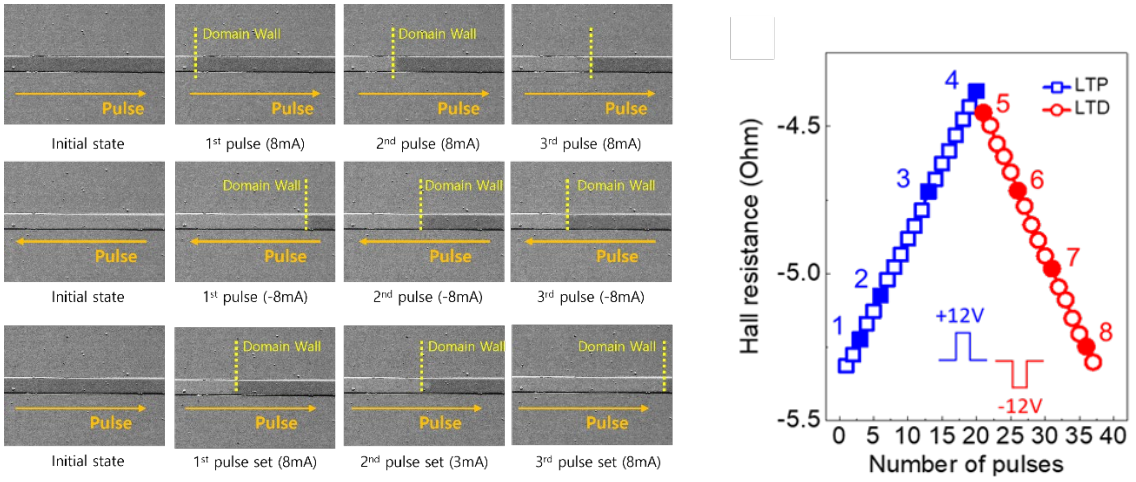

Fig1. Representative DWM by electrical pulse (left) and highly linear/symmetric variation in hall resistances (right)

Similarly, to confirm the DWM-based neuron functions as a second approach, we tried to attain a mathematical sigmoidal activation function behavior that is essential to no-trivial problem in AL network by employing the slightly different hall crossbar geometry. This device configuration was designed to have variable starting position and extremely narrow detection width in hall crossbar geometry to achieve different integrated function (I) and efficient fire function (F). It is well-known that the IF is a crucial function as a single neuron event. Fig. 2 shows the representative device configuration and their electrical pulse-driven hall resistance as a function of time. The variation in hall resistance yielded three different resistance states: inactive states, slopes, and saturation states, which clearly validated the mathematical sigmoid function that we wanted to achieve experimentally. That is, as seen in Fig. 2c, the hall resistance is unaffected until the DWM reaches the Hall detection region which is called as inactive state. The hall resistance starts to increase from state 4, reflecting the sources of nonlinearity and then followed by the saturation of hall resistance after state 7 is reached upon consecutive voltage pulses. These DWM characteristics provided one example of a basic neuron function. Our experimental findings supports that other Al device parameters including the velocity, detection, and starting positions, can be precisely adjusted by changing diverse operation parameters and the device architecture.

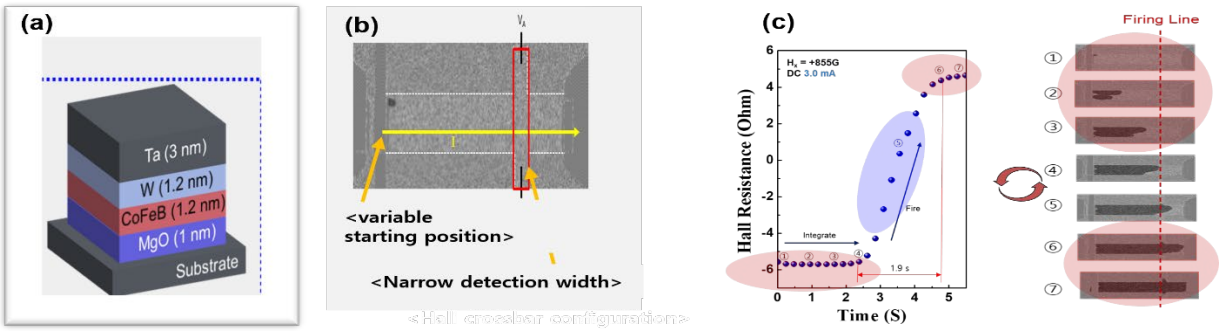

Fig2. (a) Sample stacks, (b) representative hall crossbar device configuration, (c) hall resistance variation as a function of time confirming a mathematical sigmoid function slope (blue color) and their corresponding MOKE images monitored at each number.

As a third approach, we prepared a sandwiched synthetic antiferromagnetic system (S-SyAF) of a CoFeB (FM)/W (HM)/CoFeB (FM) stack. As seen in Fig. 3a, this geometry was supposed to enable the middle HM layer to generate opposite spin currents (up and down) directed toward the top and bottom FM layers upon the application of electric current with the Ruderman-Kittel-Kasuya-Yosida (RKKY) interaction, thus ensuring an anti-ferromagnetism (AF) as specific middle W layer. That is, a proper manipulation of the RKKY interaction implements distinct oscillation exchange coupling between ferromagnetism and anti-ferromagnetism between the two FM layers due to RKKY interaction, and thus facilitates efficient reduction of the total magnetization (Fig. 3c).

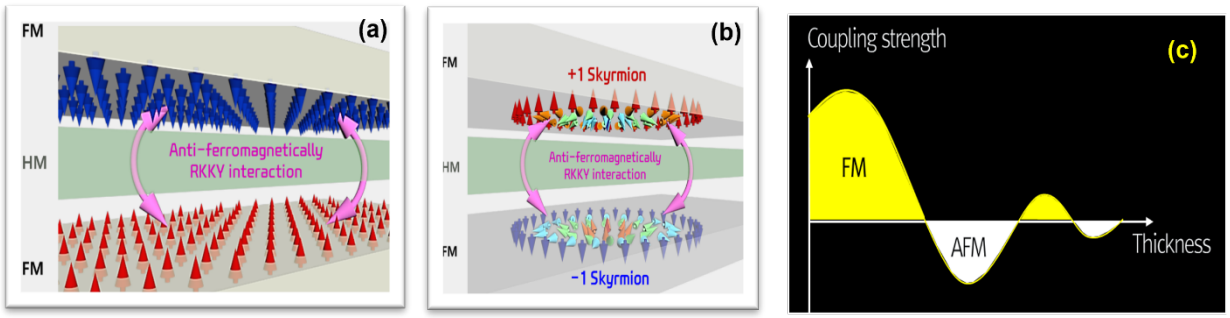

Fig3. (a) Sandwiched synthetic antiferromagnetic system, (b) possible generation of opposite spins, and (c) RKKY interaction-driven oscillation exchange coupling between ferromagnetism and anti-ferromagnetism.

Fig. 4a illustrates the representative S-SyAF stacks of MgO (1 nm)/CoFeB (1.3 nm)/W (2 nm)/CoFeB (1.3 nm)/MgO (1 nm)/Ta (3 nm) on a SiO_2 substrate, along with the hall-crossbar configuration (Fig. 4b). Fig. 4c plots the representative magnetic hysteresis loop for the z-component magnetization versus the z-axis external magnetic field (H_z), depending on the thickness of W middle layer. As seen, the antiferromagnetically coupled behaviours at a particular W thickness range (blue dashed line) was clearly observed, thus providing direct evidence of the presence of anti-ferromagnetisms. 2 nm in this study). The experimental results verified the presence of RKKY interaction between two FM layers separated by the middle non-magnetic electrode. Thus, the antiferromagnetic RKKY interaction providing he antiparallel magnetization alignment of the top and bottom FM layers reflected the possibility for the generation of near-future antiferromagnetically

coupled skrymion pairs (AFC-SkPs), along with attaining the possible nature of skyrmion generation. Fig. 4d presents the W thickness dependent M-H curves.

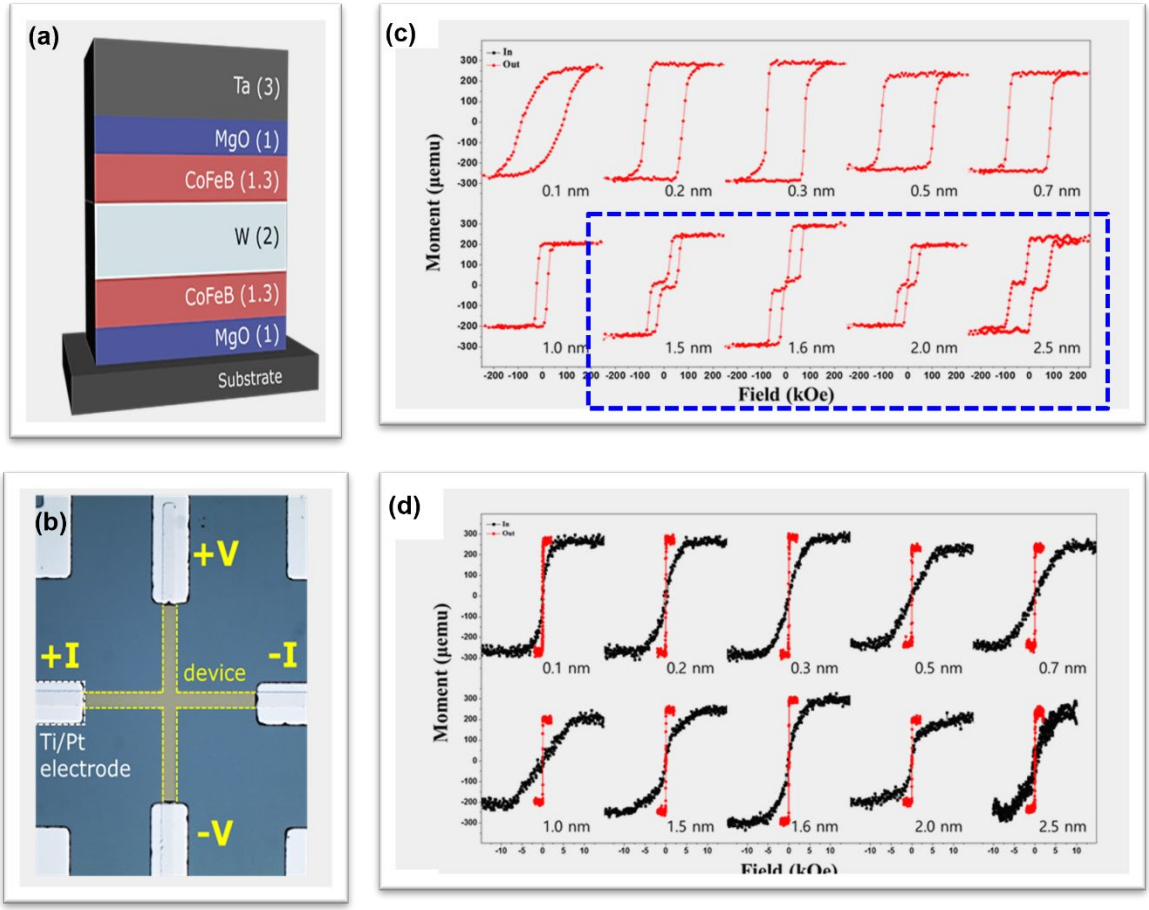

Fig4. (a) Schematics of sample stacks, (b) hall crossbar configuration for measurements, (c) Oscillating exchange coupling between FM and AFM, and (d) Sandwiched synthetic antiferromagnetic system, (b) possible generation of opposite spins, and W thickness dependence of magnetization.

As a fourth approach, we studied the magnetic strip patterns between spin-up and spin-down domains observed from the ferromagnetic film itself since attaining a firm understanding of their physical nature remains a key starting step towards extending their use in efficient skrymion generation. In general, nature provides various two-dimensional (2D) physical stripe domain patterns of order parameters. In addition, it is well-known that the generation of diverse strip patterns has a universal mechanism: the competing interaction between short-range interaction favoring uniform states and long-range interactions favoring mixed states. In particularly ferromagnetic materials of this work, a perpendicularly magnetized system prefers the magnetization vector between up or down

magnetization directions only, reflecting that the order parameter of magnetic strip pattern is a magnetization along the easy axis. Thus, we expect that the short-and long-range interaction in this system comes from the well-known Heisenberg exchange and dipole–dipole interaction, respectively. The Heisenberg exchange interaction favors parallel alignment of two neighboring spins over the infinitely wide domain, while the dipole–dipole interaction favors a perfectly mixed state with the smallest domains for minimizing the demagnetization fields between adjacent domains. Recent work addressed that efficient generation or manipulation of magnetic skrymion is highly dependent on the reduction of PMA energy or enhancement of DMI energy contribution, as mentioned in previous equation of (1). Thus, to understand/validate the competition interaction for determination of uniform magnetic domains and magnetic stripe domain pattern width, we prepared the similar stacks of SiO2 (200 nm)/W (5 nm)/CoFeB (1.3 nm)/Ta (0.10–0.14 nm)/MgO (1 nm)/Ta (1 nm) with perpendicular magnetic anisotropy characteristics (PMA). In particular, the edge-type Ta thin layer was inserted between the CoFeB/MgO interfaces to possibly deteriorate the PMA strength as our first approach since intentional enhancement of DMI energy was not clear at this moment.

Fig. 5 shows the representative Ta layer-inserted sample stacks and their corresponding MOKE images for magnetic strip pattern in a perpendicularly magnetized system, where a proper insertion in sample stack was supposed to strongly affect the PMA characteristics between CoFeB and MgO interfaces. As seen in the MOKE image, the light and dark grey regions represented + z and (- z) magnetization domains of perpendicularly magnetized system, along with variation in strip domain width that depends on the thickness of Ta layer (0.1 and 0.2 Ta thickness).

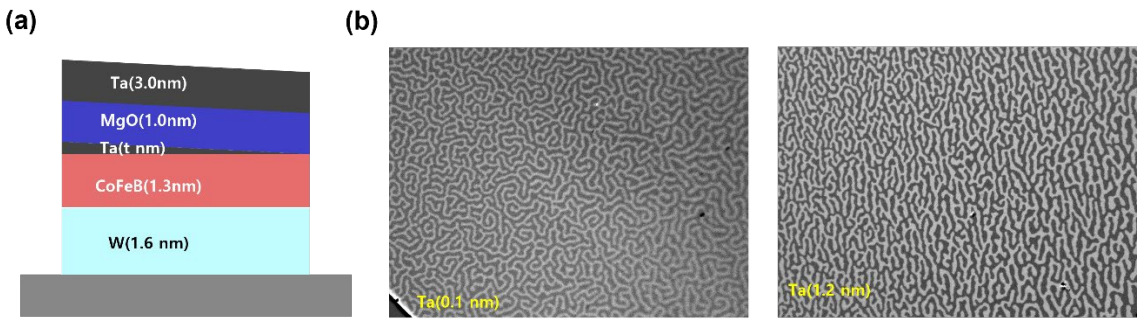

Fig. 5. (a) Schematics of Ta layer-inserted sample stacks, (b) representative MOKE images monitored for 0.1 and 0.2 nm thick Ta layer. As expected, slightly different strip pattern domains and widths were observed.

Since the stripe domain width is highly associated with on material/operation parameters, and device geometries, variation in stripe pattern width was also tested by changing in-plane magnetic field (H_x) as one operation parameter, as evident in Fig. 6

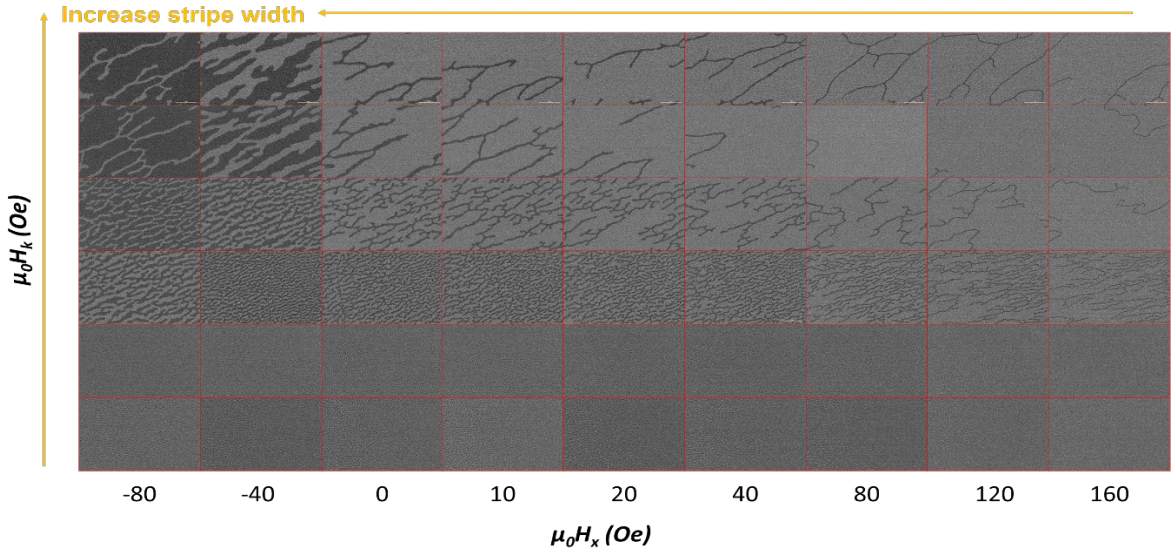

Fig. 6. Variation in strip pattern domain and widths, depending on magnetic field amplitude of H_x

As displayed in Fig. 6, the stripe pattern domain and width increase with an increase in H_x, which is directly related to the domain wall energy; that is, introducing a high domain wall energy causes the domain wall density to be reduced, thus supporting increase in stripe width. These initial experimental results suggest that thin or thick strip pattern width can be precisely adjusted by choosing operation parameters. With the observations of magnetic strip pattern, we are now focusing on determining the exact transition nature from the magnetic strip patterns to skyrmion generation by optimizing device geometry and operation parameters because the specific stripe form achieved by the competition between the domain wall energy comprising short-range interaction and PMA, and the dipole energy directly will be the consequence of skyrmion generation under applied electrical pulse. Fig. 7 plots the other example of the magnified strip pattern domain and width in the range of 0.09 to 0.11 nm thick-

Ta inserted layer, indicating that precise manipulation of PMA energy reduction is highly needed to attain a suitable strip pattern and their corresponding generation of skrymion.

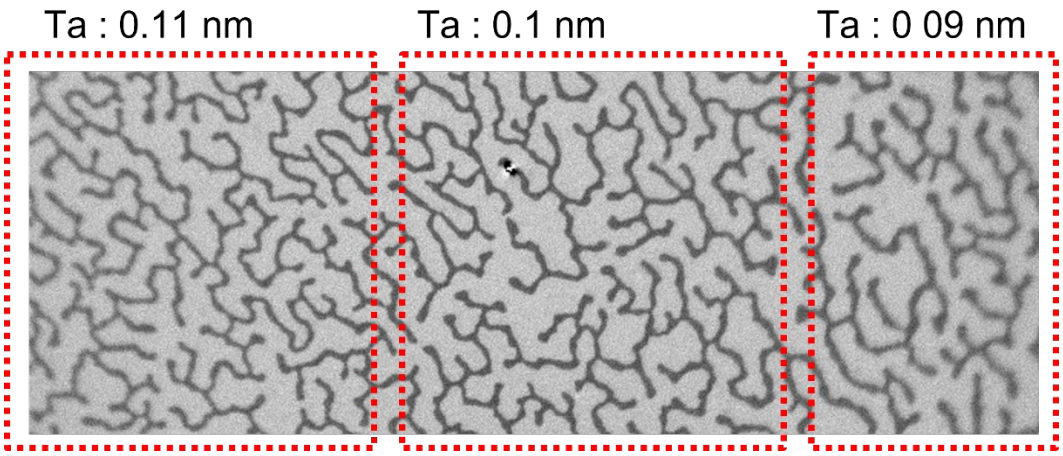

Fig. 7. Other example for variation in strip pattern domain and widths in an extremely small Ta insertion range thickness

IV. SUMMARIZED ACCOMPLISHMENTS FOR 2nd YEAR

In the second year of this study, research was conducted with three main objectives. Firstly, we conducted foundational research on the dynamics of domain wall dynamics and the application of future Al device by extending current results to skyrmion pair dynamics. This involved the creation of various devices in a triple-layered RKKY structure consisting of ferromagnetic layer (FM1), metal (HM), and another ferromagnetic layer (FM2). By altering the thickness of the intermediate metal layer, we aimed to manifest AFM exchange interchange coupling. Secondly, we sought to understand domain wall dynamics in the established AFM-RKKY structure under the influence of external magnetic fields and current. Specifically, in the AFM-RKKY structure, we analyzed and compared the effects of AFM and DMI to determine the dominant influence on DWM dynamics.

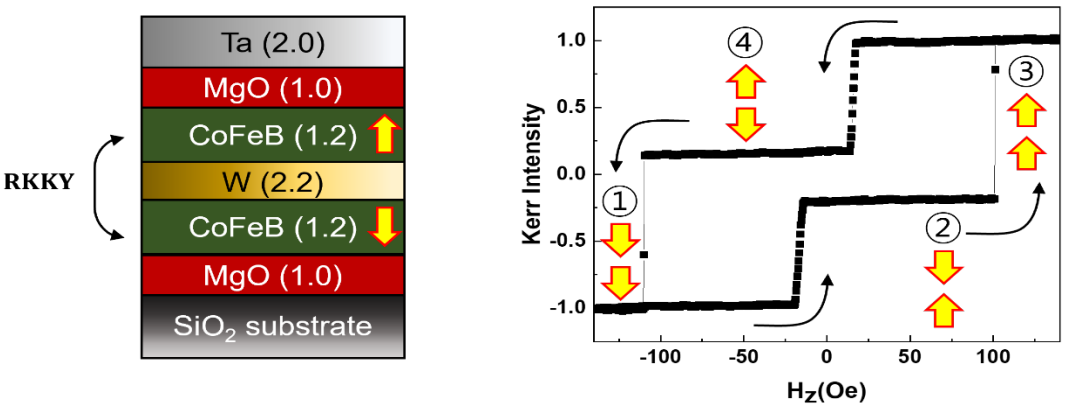

Fig. 1. Triple-layered RKKY structures (Left) and Fig. 2 Their MOKE measurements (Right).

Figure 1 depicts a representative triple-layered RKKY structure consisting of ferromagnetic layer (FM1), heavy metal (HM)- ferromagnetic layer (FM2) aimed at providing RKKY properties. We attempted to realize both FM and AFM exchange interchange coupling by varying the thickness of the intermediate heave metal (HM) layer in this RKKY structure. Figure 2 presents the MOKE (Magnetic Optic Kerr Effect Microscopy) measurement results for the RKKY multilayer structure. As

demonstrated in the figure, the RKKY structure exhibits antiferromagnetic coupling (AFM) phenomena at an appropriate HM thickness. Specifically, it displays four distinct magnetization orientations between the top and bottom ferromagnetic layers when an external magnetic field is applied. For instance, applying a sufficiently large negative external magnetic field aligns the magnetization directions of both top and bottom ferromagnetic layers downwards (①). As this external field increases, the magnetization direction of the bottom ferromagnetic layer switches to upwards, resulting in an antiparallel coupling of the two FM layers. The bottom FM layer switches first due to its comparatively smaller magnetization magnitude after material growth. However, even if the top layer were to switch its direction first, it would not pose a problem. In the RKKY structure, a tungsten (W) layer serves as the heavy metal layer, acting as a spacer layer in the RKKY structure. It supports the growth of CoFeB ferromagnetic films on both its top and bottom, and the formation of RKKY antiferromagnetic coupling has been observed, as seen in this figure. Notably, with an external magnetic field of 0 Oe, if the magnetization direction of the CoFeB ferromagnetic layer above the W middle layer is upwards, the CoFeB layer below the W points downwards.

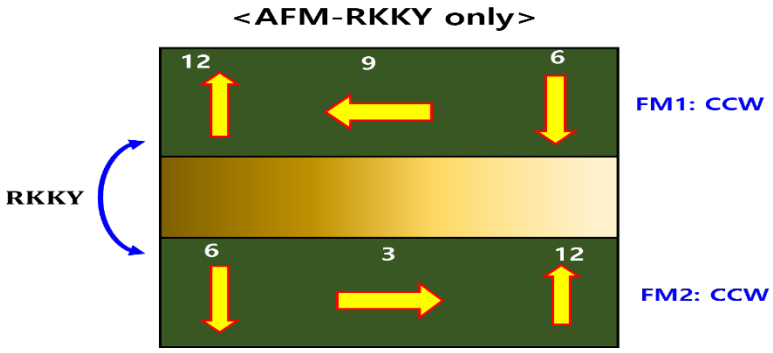

Fig. 3. Magnetization direction combination between two ferromagnetic layers by considering AFM-RKKY effect.

In multilayer structures combined with RKKY properties, two physical phenomena need to be considered when switching the magnetization direction of the top and bottom FM layers under external magnetic fields or current application. Specifically, they are the antiferromagnetic coupled-RKKY (AFM-RKKY) phenomenon occurring between the ferromagnetic layers at specific W

thickness and the DMI effect occurring at the interface of the FM layer and the HM intermediate layer. Figure 3 schematically represents the magnetization switching direction of the top and bottom FM layers by considering only the AFM-RKKY phenomenon. Firstly, the magnetization directions of the FM layers in a multilayer structure must form in opposite directions due to the AFM-RKKY phenomenon. For instance, if we assume that during an external magnetic field or current application, the top FM's magnetization switching direction rotates counterclockwise (CCW: 12->9->6 o'clock) as depicted in the figure, the bottom layer's magnetization switching direction should rotate from 6->3->12 o'clock. Hence, the magnetization direction of the bottom FM layer must be in the same CCW direction as the top layer's magnetization switching direction. Further explaining through Figure 3, considering only the magnetization direction of the intermediate domain within the top and bottom FM layers, if the top FM layer's intermediate domain has a 9 o'clock magnetization direction, the bottom FM layer's intermediate domain magnetization direction should be at 3 o'clock then due to the AFM-RKKY phenomenon. Consequently, the overall magnetization switching direction of the bottom FM layer becomes CCW. The results imply that both the top and bottom FM layers exhibit a CCW magnetization switching direction.

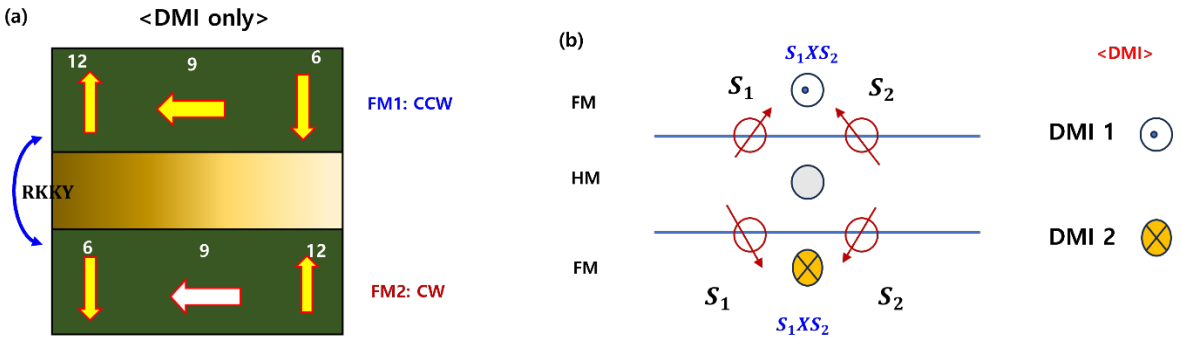

Fig. 4. (a) Magnetization switching direction of the top and bottom FM layers by considering only the DMI effect occurring at the FM/HM interfaces and (b) DMI vector indications.

Figure 4a illustrates the magnetization switching direction of the top and bottom FM layers by considering only the DMI effect occurring at the FM/HM interfaces. For example, in a FM-HM-FM

triple RKKY structure, the top and bottom FM layers form two distinct interfaces with the centrally located HM. Thus, two DMI effects should be considered in this work. Figure 4b schematically represents the DMI effect emanating from the plane of the figure due to $\boldsymbol{S_1 X S_2}$ at the FM/HM interface of the top ferromagnetic layer in the 3-layer multi-layered structure, and the DMI effect entering into the plane of the figure due to $\boldsymbol{S_1 X S_2}$ at the bottom HM/FM interface. Therefore, when considering the two DMI effects, if the magnetization switching direction of the top FM layer is counterclockwise (CCW), the magnetization switching direction of the bottom FM layer forms a clockwise (CW) direction due to the DMI effect, as shown in Figure 4a. Hence, one can anticipate that in the bottom FM layer, the magnetization switching directions due to the AFM-RKKY phenomenon (CCW) and the DMI effect (CW) counteract each other. That is, when an external magnetic field or current is applied, determining the magnetization switching direction of the bottom FM layer in the RKKY structure requires simultaneous consideration of both AFM-RKKY and DMI effects.

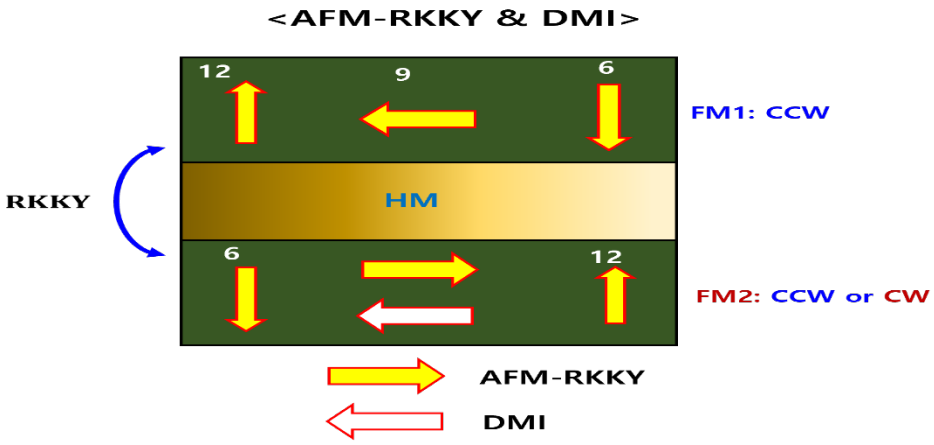

Fig. 5. Predicted magnetization switching direction under AFM-RKKY or DMI effects.

Figure 5 schematically represents the predicted results of the magnetization switching direction in the ferromagnetic layer of the RKKY structure, influenced by both the AFM-RKKY and DMI effects.

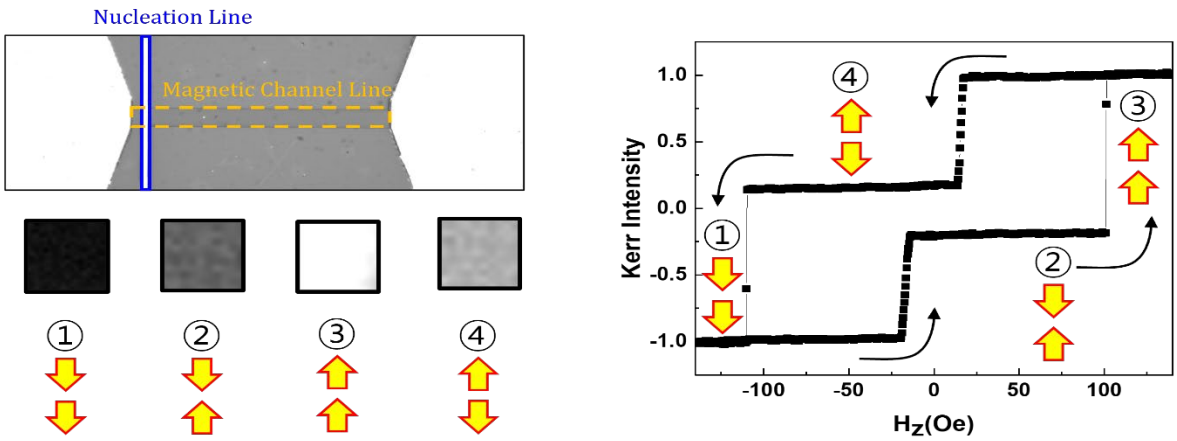

Fig. 6. magnetic orientation combinations of the top and bottom FM layers measured by MOKE

Figure 6 illustrates the magnetic orientation combinations of the top and bottom FM layers in a triple-layered RKKY structure, measured via MOKE after the application of an external magnetic field in the Hz direction. For this measurement, a RKKY multilayer films were grown, subsequently processed into a Hall-bar structure, and the MOKE images of the magnetic orientations of the top and bottom FM layers were captured as the magnitude of the external magnetic field in the Hz direction was varied. When a large negative external Hz magnetic field is applied, the magnetic orientations of both FM layers align in an all-down magnetic direction (①), represented by an entirely black MOKE image. Conversely, upon the application of a large positive external magnetic field, the magnetic orientations of both layers align in an all-up magnetic direction (③), producing a white MOKE image. For the two FM layers where AFM-RKKY properties are present, the magnetic orientations of the top and bottom FM layers are formed in opposite directions, resulting in a MOKE image that is a blend of black and white. For instance, combinations of down-up magnetic orientations (②) and up-down magnetic orientations (④) in the two FM layers produce similar MOKE images. However, slight image differences arise since the magnitudes of the magnetizations in the top and bottom FM layers are somewhat different. Although both combinations display similar AFM-RKKY induced magnetic orientations, there can be subtle variations in the MOKE images.

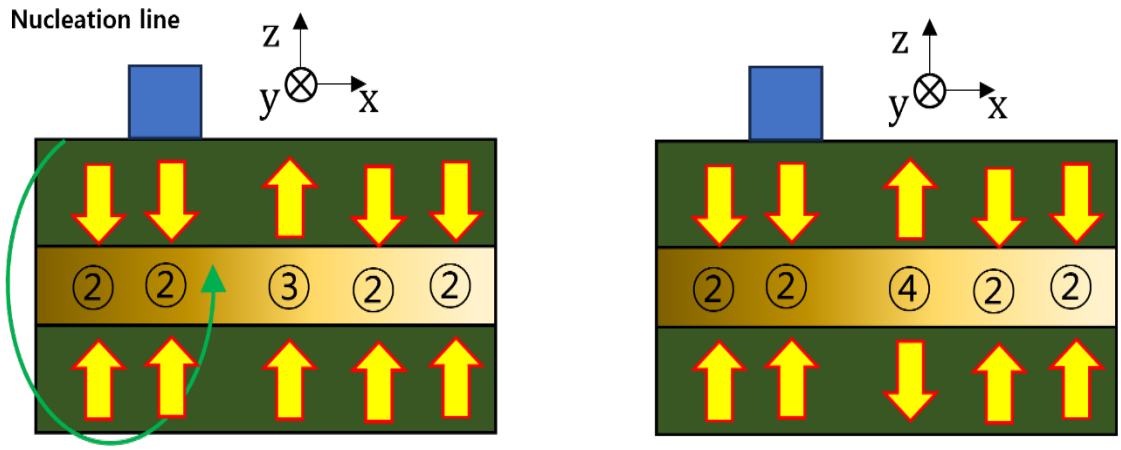

Fig. 7. Magnetization combination of the top and bottom FM layers under external current

Figure 7 illustrates the cross-sectional structure of a Hall bar with an additional nucleation line. This is designed so that when a current is applied externally through the nucleation line, it artificially modifies the magnetic direction combination of the top and bottom FM layers. For instance, when the two FM layers initially have a down-up magnetic alignment, as seen in state ②, applying a sufficient current in the -y direction through the nucleation line can switch the magnetization direction of both FM layers to produce an up-up alignment, as in state ③. Consequently, while the upper FM layer retains its up-magnetization, the lower FM layer, influenced by the AFM-RKKY property, adopts a down-magnetization, culminating in an up-down alignment in state ④ upon external current application. Measurements via MOKE have confirmed that the magnetization magnitude of the upper FM layer exceeds that of the lower layer, signified as $M_{upper}>M_{lower}$.

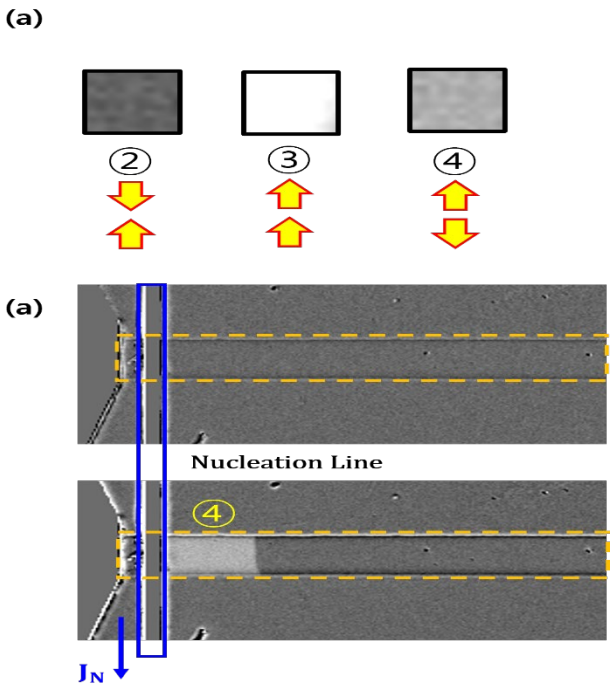

Fig. 8. MOKE images of a device incorporating a nucleation line within the Hall-bar structure and image extension.

Figure 8 displays optical and MOKE images of a device incorporating a nucleation line within the Hall-bar structure, designed for the application of external current. Figure 8a shows the MOKE image illustrating the combinations of magnetic orientations formed between the two FM layers.. Figure 8b depicts an image showing the shift in the magnetic orientation of the FM layer due to the magnetic field generated upon applying an external current through the nucleation line in an AFM-RKKY structure. For instance, when an external current is applied through the nucleation line, it produces a magnetic field in the +z direction around the line according to Ampère's Law. Hence, we can observe that the initial down-up magnetic orientation combination (②) of the two FM layers eventually shifts to an up-down combination (④, white MOKE image) due to the magnetic field induced by the external current. This demonstrates that the combination of magnetic orientations in FM layers can change indirectly as a result of the applied magnetic field.

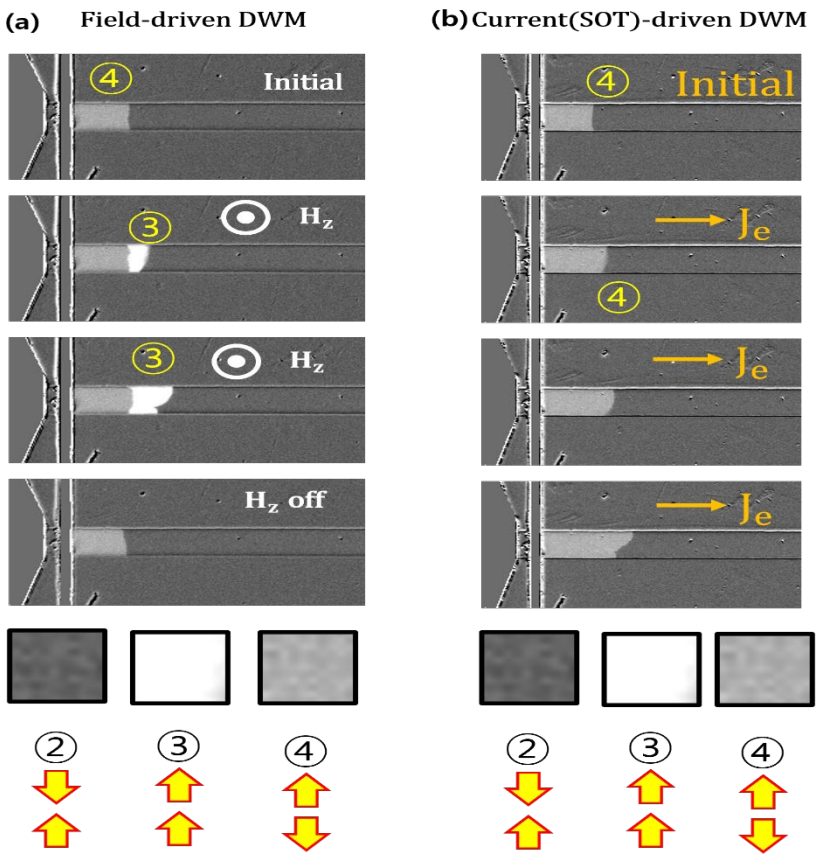

Fig. 9. (a) Field-driven DWM and (b) Current-driven DWM MOKE images

Generally, in ferromagnetic materials, domain wall motion (DWM) can be achieved by applying an external magnetic field or current. Thus, in this study, to understand the magnetic switching phenomena for DWM in triple layered RKKY structures, we considered two potential properties: AFM-RKKY and DMI effects. We analyzed and compared the influence of the external magnetic field-induced DWM and the current-induced spin-orbit torque (SOT) based DWM to ascertain which property has the dominant effect. Figure 9 displays the representative changes in MOKE images due to DWM under external magnetic fields and applied currents. Figure 9a depicts the variations in DWM MOKE images with the application of an external magnetic field. This is labeled as field-driven DWM. When an external current is applied using the Nucleation line, a magnetic field arises due to Ampere's Law. This magnetic field transforms the initial state of the down-up magnetic orientation (②) to the up-down magnetic orientation (④). The figure represents results of MOKE measurements taken

during the application of an external magnetic field in the +**z** direction, monitoring the DWM alteration. In Figure 9a, the field-driven DWM, initially driven by AFM-RKKY, causes the two vertically adjacent FM layers to form in the up-down magnetic orientation (④). When an external magnetic field from the +**z** direction is applied to this initial state, the down magnetization orientation in the lower FM layer changes to up, resulting in an up-up magnetization orientation (③). Consequently, the MOKE image turns white when the +$\boldsymbol{Hz}$ external magnetic field is applied. As the external magnetic field continues, the domain with the up-up magnetization orientation (③) expands, and as shown in Figure 9a, the white MOKE image area increases. However, upon removal of the +$\boldsymbol{Hz}$ external magnetic field, the magnetization orientations of the two FM layers revert to their initial up-down orientation (④) under the influence of AFM-RKKY. Figure 9b presents the DWM MOKE images corresponding to an externally applied current, denoted here as current-driven DMW. The initial state aligns closely with the field-driven DMW in Fig. 9a, where the magnetization directions of the upper and lower FM layers are formed as up-down (④) orientations due to the AFM-RKKY interaction. Upon applying a current $\boldsymbol{Je}$ in the +**x** direction, a DWM is induced as a result of the Spin-Orbit Torque (SOT) phenomenon. As illustrated, with the external current application, the original up-down magnetization orientation (④) is maintained, and the initial region progressively expands. This indicates that in the RKKY structure, the external current-induced DWM doesn't alter the initial magnetization combination of the two FM layers. This experimental outcome contrasts with the results from the field-driven DWM.

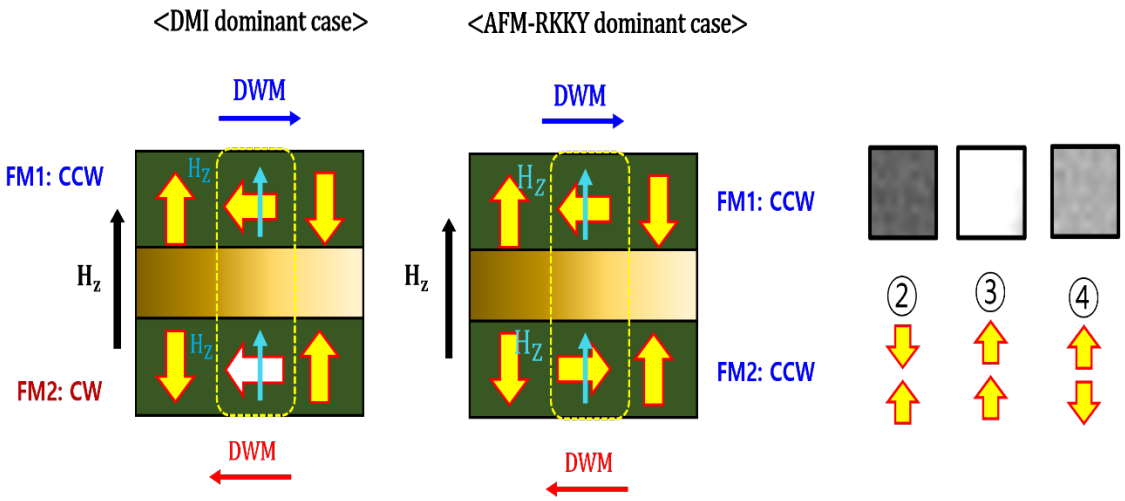

Fig. 10 Schematic of the field-driven DWM under DMI (Left) and AFM-RKKY (Right) effects.

Figure 10 illustrates a schematic of the field-driven DWM to elucidate the fundamental nature of the differences between two distinct experimental outcomes. Firstly, in scenarios where the DMI influence predominates, as depicted in the anticipated schematic, upon applying an external magnetic field $+\boldsymbol{Hz}$ to the up-down magnetization combination (④) of the two superimposed FM layers, the DW of the top FM layer shifts to the right, while the DW of the bottom layer expands to the left. Consequently, in the intermediate region, both top and bottom FM DMs establish a mutual up-up magnetization alignment, leading to an expanding white MOKE region (③) in the MOKE image as the external magnetic field is applied. Similarly, in the schematic dominated by AFM-RKKY effects, upon applying the external magnetic field $+\boldsymbol{Hz}$ to the up-down magnetization alignment combination (④), the DW of the top FM layer moves to the right, while that of the bottom FM layer broadens to the left. As a result, both top and bottom FM DMs in the intermediate area attain the same up-up magnetic direction. Thus, the white area in the MOKE image progressively enlarges. In conclusion, MOKE images based on DWM due to an external magnetic field are predicted to enhance the up-up magnetic alignment region, irrespective of whether the AFM-RKKY or DMI effect is more pronounced.

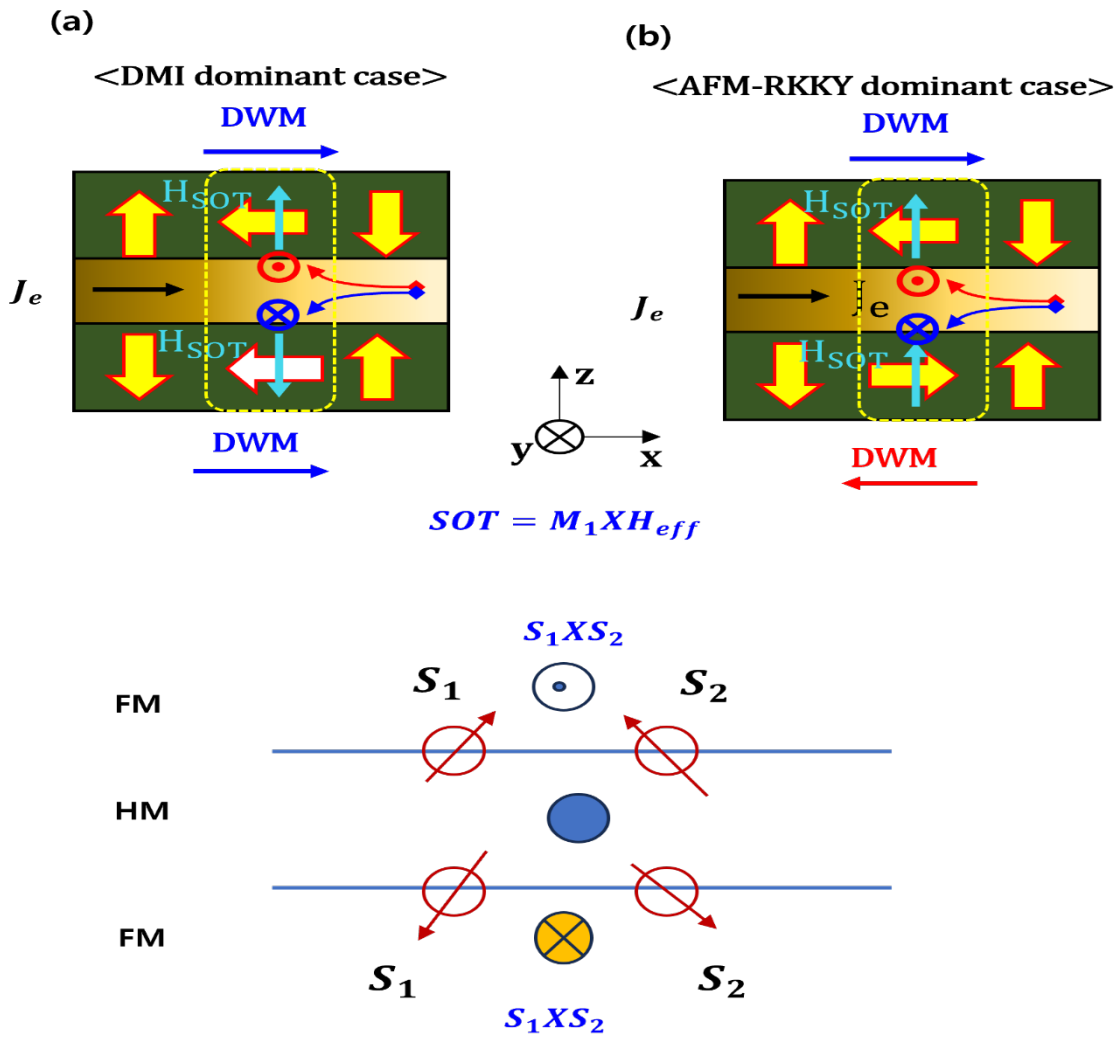

Fig. 11 Schematic of a current-driven DWM under DMI (Left) and AFM-RKKY (Right) effects

Figure 11 illustrates the schematic of a current-driven DWM induced by an external current. As depicted, when an external current is applied to the triple-layered RKKY structure, the majority of the current flows through the middle layer, W HM. Therefore, the influence of the current-driven SOT-DWM can be considered in two scenarios. When a current is applied in the +x direction on the RKKY structure, electrons move in the opposite direction, −x. Within the W layer, a spin-orbit-coupling (SOC) phenomenon occurs, causing the electrons' spins to separate into up-spin and down-spin. These spins then migrate to the top and bottom FM layers, forming spin currents in +y and −y directions, respectively. Consequently, the distinct spin current-driven SOT effects on DWM can be contemplated in two contexts: DMI and AFM-RKKY. Figure 11a presents a scenario dominated by

DMI. In this situation, the DW of the upper FM layer is influenced by the +y spin current, causing SOT to act in the +z direction. As a result, the DW expands to the right. Similarly, the DW of the lower FM layer, influenced by the −y spin current, also undergoes SOT in the +z direction and expands rightward. Taking into account the magnetization direction in the central region, it can be inferred that the initial up-down magnetization orientation is maintained, suggesting DWM progression. Hence, when a dominant DMI effect is present during external current application, the initial MOKE image is anticipated to grow progressively. Figure 11b portrays a condition where AFM-RKKY predominates. Here, the DW of the top FM layer, under the influence of the +y spin current, experiences SOT in the +z direction, leading it to widen to the right. However, the DW of the bottom FM layer, affected by the −y spin current, undergoes SOT in the +z direction and broadens to the left. Considering the magnetization orientation in the intermediary region, the DW shifts from an up-down to an up-up state. Thus, the MOKE image should turn white when current is applied due to DWM. Comparing both scenarios and observing that the initial magnetization direction remains unchanged in MOKE image measurements, it can be deduced that the DWM induced by the external current is primarily influenced by the DMI effect.

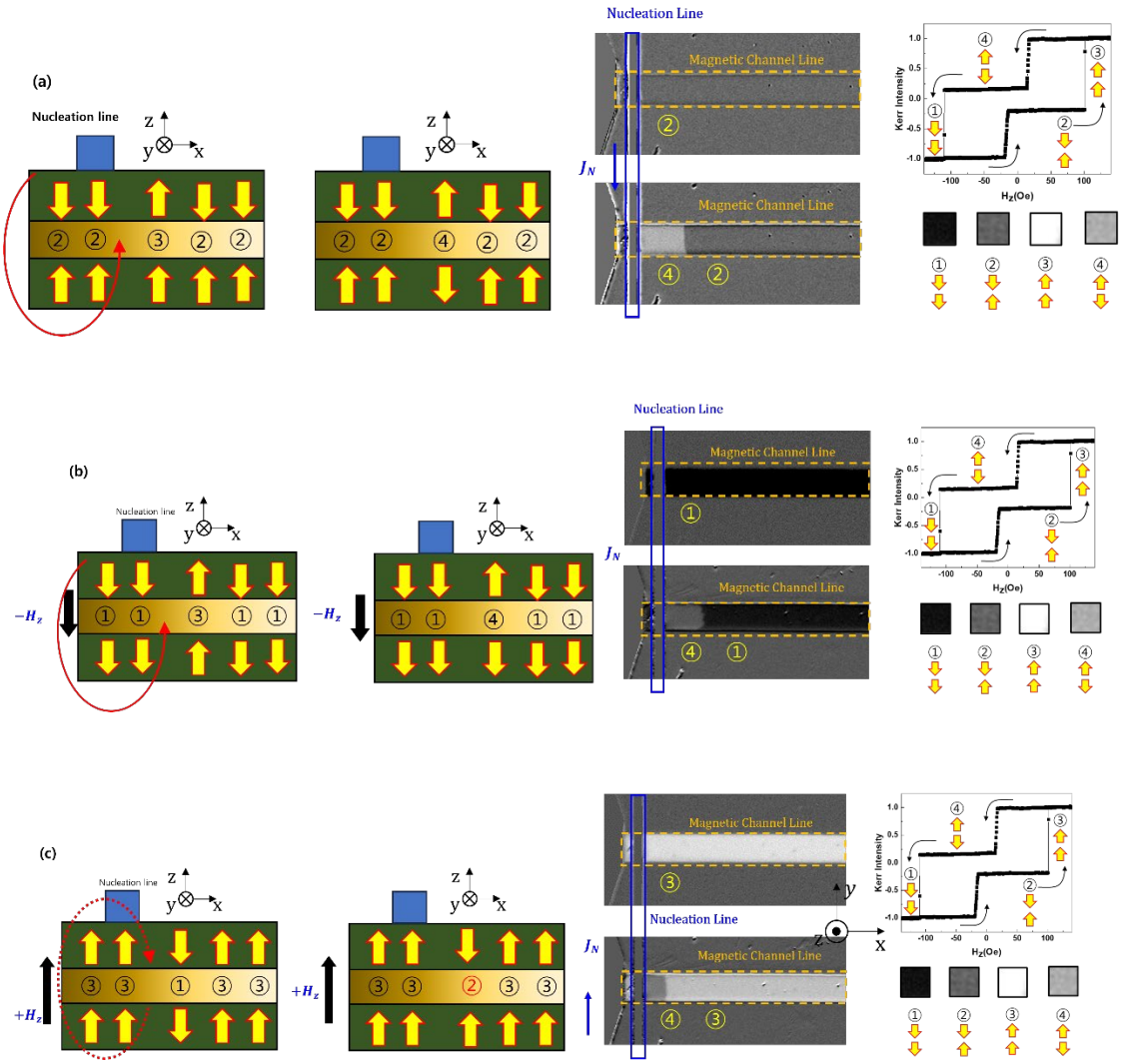

Fig. 12. (a) AFM-RKKY, (b) Upper-single RKKY, and (c) Lower-single RKKY configurations and their MOKE images.

To clarify the DWM speed induced by an external magnetic field in a triple-layered RKKY structure, three configurations were initially fabricated based on the presence or absence of an external magnetic field: the AFM-RKKY, Upper-single RKKY, and Lower-single RKKY. Figure 12a depicts the schematic of how the AFM-RKKY DW is formed. Initially, it shows the change in the magnetization combination of the upper and lower FM layers when an external current is applied through the Nucleation line. From its original state, marked as ②, which has a down-up magnetization direction combination, applying a sufficient external current J_N in the -$\boldsymbol{y}$ direction through the Nucleation line can transform the adjacent magnetization directions into the up-up combination,

marked as ③. Notably, prior knowledge from MOKE measurements informs us that the magnetization magnitude of the upper FM layer is larger than that of the lower one. Thus, while the upper FM layer retains its up-magnetization direction due to its AFM-RKKY properties, the lower FM layer, having a smaller magnetization magnitude, assumes a down direction. Consequently, when an external current is applied, a magnetization direction combination of up-down, marked as ④, is formed. This prediction was validated by observing the formation of an image of the ④ state in the magnetic channel line through MOKE measurements. Figure 12b illustrates the schematic for the formation of the Upper-single RKKY magnetization. Initially, an external magnetic field, $-\boldsymbol{Hz}$, is applied, orienting the magnetization direction of the two antiferromagnetically coupled FM layers to a down-down combination, denoted as state ①. When an external current (J_N) is applied in the $-\boldsymbol{y}$ direction through the Nucleation line during the ① state, the ensuing Oersted field induces a switching of the domain in the FM layer adjacent to the nucleation line, transforming it to the state ③ with an up-up magnetization combination. Consequently, while the upper FM layer retains its up-magnetized state, the lower layer's domain, which possesses a weaker magnetization due to the AFM-RKKY property, assumes a down direction. This leads to the eventual formation of state ④, characterized by an up-down magnetization direction combination. This predicted outcome was verified through MOKE measurements, where the state ④ image was observable in the magnetic channel line upon external current application. Figure 12c illustrates a schematic for the formation of lower-single RKKY magnetization. Initially, an external magnetic field in the $+\boldsymbol{Hz}$ direction is applied to align the magnetization direction of the two vertically stacked FM layers to an up-up configuration, denoted as state ③. When an external current J_N is applied in the $+\boldsymbol{y}$ direction through the nucleation line in the magnetization combination of state ③, the resulting Oersted field causes the magnetization direction

of the FM layers adjacent to the nucleation line to switch, transitioning to the down-down magnetization combination, labeled as state ①. As mentioned earlier, magneto-optical Kerr effect (MOKE) measurements indicate that the magnetization magnitude of the upper FM layer is larger than that of the lower layer. Thus, the domain of the upper FM layer retains its down-magnetization direction, while, due to the AFM-RKKY property, the domain of the lower FM layer switches to the up direction. Consequently, upon the application of external current, the magnetization combination maintains its down-up direction, denoted as state ②, with an expanding region. This expansion of the state ② region can be confirmed through MOKE measurements. In summary, the MOKE measurements verify the expansion of the MOKE image in the state ② upon the application of external current in the magnetic channel line.

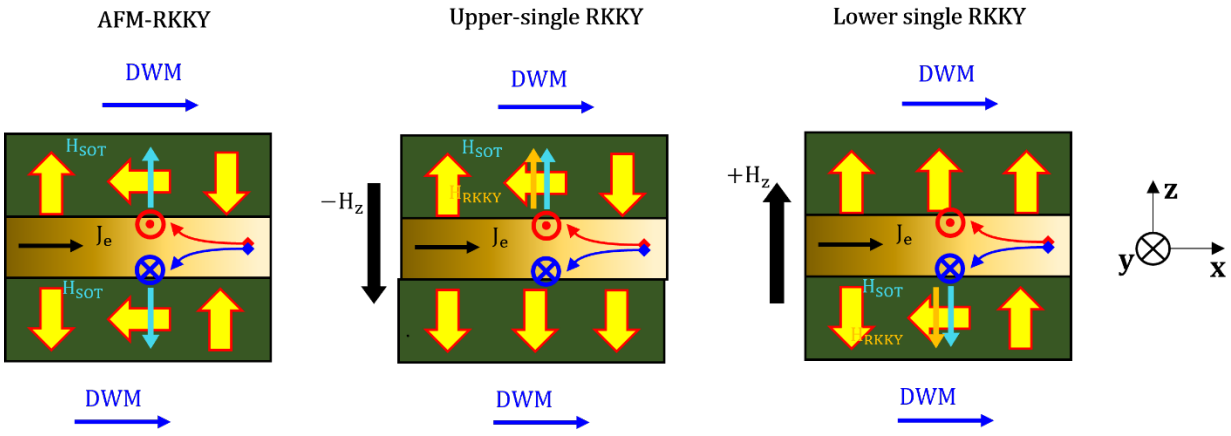

Fig. 13. Magnetization switching of AFM-RKKY, Upper-single RKKY, and Lower-single RKKY configurations under external currents.

In structural terms, if an external magnetic field is not applied initially, the AFM-RKKY phenomenon in its initial state is maintained. When an external magnetic field is applied in the -***Hz*** direction, an upper single RKKY (u-RKKY) structure forms, wherein the magnetization direction of the underlying FM layer is entirely downward. On the other hand, applying an external magnetic field

in the $+\boldsymbol{Hz}$ direction results in the transition to the lower single RKKY (L-RKKY) structure. Hence, from an artificially formed triple-layered RKKY structure, if an external current is applied in the $+\boldsymbol{x}$ direction, as depicted in Figure 13, it is anticipated that the domain walls (DWs) of both the upper and lower FM layers will move to the right.

In conclusion, with these observations, the DWM speeds will become systematically analyzed across the three structures as possibly new projects and for understanding future skyrmion pair dynamics, which can be generated by understanding the possible nature of domain wall motion or velocities in triple-layered RKKY structures

V. EXPANDED ACCOMPLISHMENTS

Recently, the spin-orbit switching-based reconfigurable logic devices have shown appreciable potential to provide reliable solutions for ultra-low power, high-speed, high-density, and non-volatile systems. Furthermore, the ability to attain multiple logic operations in a single chip frame possibly extends their use in better scalability and efficiency than traditional logic devices. Thus, as an expanded approach of this work, we also fabricated the multiple reconfigurable magnetic domain logic gates in a single two-channel hall bar device via voltage-driven read current directions in W/CoFeB/MgO/Ta stacks since novel spin-dynamic architectures based on magnetic domain (MD) switching phenomena are highly promising for use in fast operation speed, non-volatility, and multiple processes and store information in a single device configuration. That is, the SOT-driven MD characteristics for the implementation of eight reconfigurable spin logic gates in a single two-channel hall bar frame were initially analysed. Anomalous hall effect (AHE) voltages were monitored by employing different variations in circuit connection for analyses. At first, similar sample stacks of Si/SiO2/2 nm W/2 nm $Co_{20}Fe_{60}B_{20}$/1.1 nm MgO/1 nm TaO_x/2 nm with perpendicular magnetic anisotropy were fabricated, as seen in **Fig. 1a**. **Fig. 1b** shows the representative hall bar configuration composed of two channels 1 and 2 highlighted in red and blue dashed boxes, respectively. The AHE voltage (V_H) mainly determined by the z component of the net magnetization was recorded across the two-channel hall

bar geometry. The symbols of V_{H1}, V_{H2}, V_{H3}, and V_{H4} (white color) were defined as the AHE voltage electrodes. The AHE voltage of each channel (V_{H13}, V_{H24}) was probed by the V_{H1}, V_{H2}, V_{H3}, and V_{H4} at the hall bar structure. The black line represented the AHE voltage (V_{H13}) of channel 1, while the red line corresponded to the AHE voltage (V_{H24}) of channel 2 **(Fig. 1c**). **Fig. 1d** illustrates the typical circuit schematic of the Hall bar structure and voltmeter (green) as a connection approach to determine the V_s.

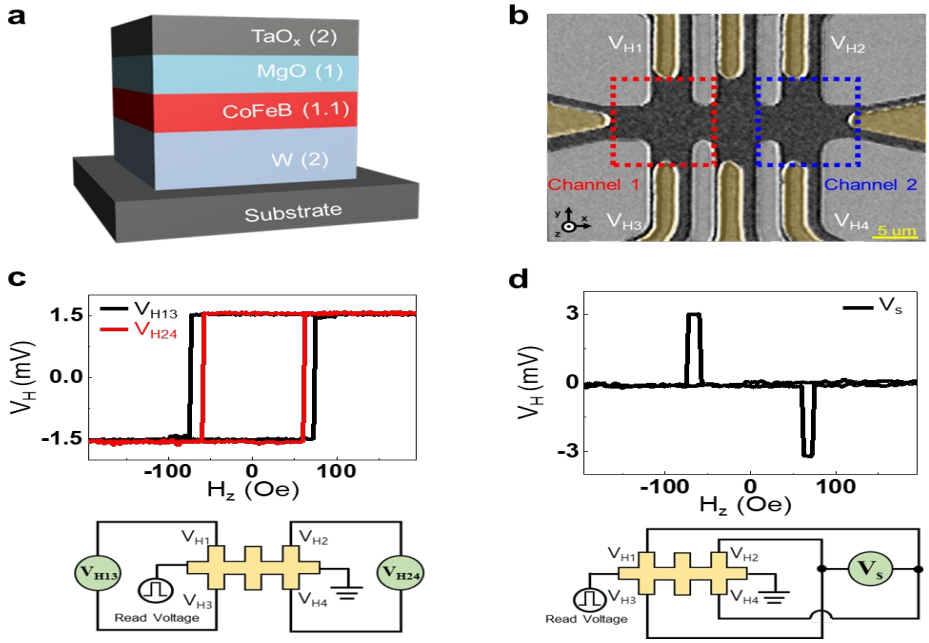

Fig. 1. (a) Device stacks, (b) Optical images of a two-channel hall bar device, along with the AHE voltage electrodes marked by V_{H1} ~ V_{H4}. (c) Hall voltage V_H verse out-of-plane magnetic field (H_z) and (d) Subtracted Hall voltage (V_s) verse out-of-plane magnetic field (H_z).

To illustrate the functions of logic gates, three experiments were conducted with different logic-input configurations (V_1, V_2), external magnetic fields (H_x), and read current (J_{read} = 1.0 x 10^6 A/cm^2) in the same structure, as seen in **Fig. 2a**. Four logic-input configurations of 'TT', 'TF', 'FT', and 'FF' were identified by applying ±10V amplitude and 100ms, where the logic-input configurations were marked by the red (V_1) and blue (V_2) bars (**Fig. 2a**). As one prominent advantage of this work, the

time-synchronization for the MDs is not required owing to their non-volatile behaviors of MDs. Input V_1 was first applied, and after an interval of 10ms, input V_2 was applied and we subsequently applied another small read voltage pulse (1V, 100ms) at the end of which AHE voltage was observed. The displayed ⓝ represented each interval at which the logic inputs were applied, as shown in **Fig. 2a**; the corresponding MD in each subtracted Hall voltage state was also given by the MOKE images (**Fig. 2b**). This spin-orbit driven logic functions are under going as the other example of extra work.

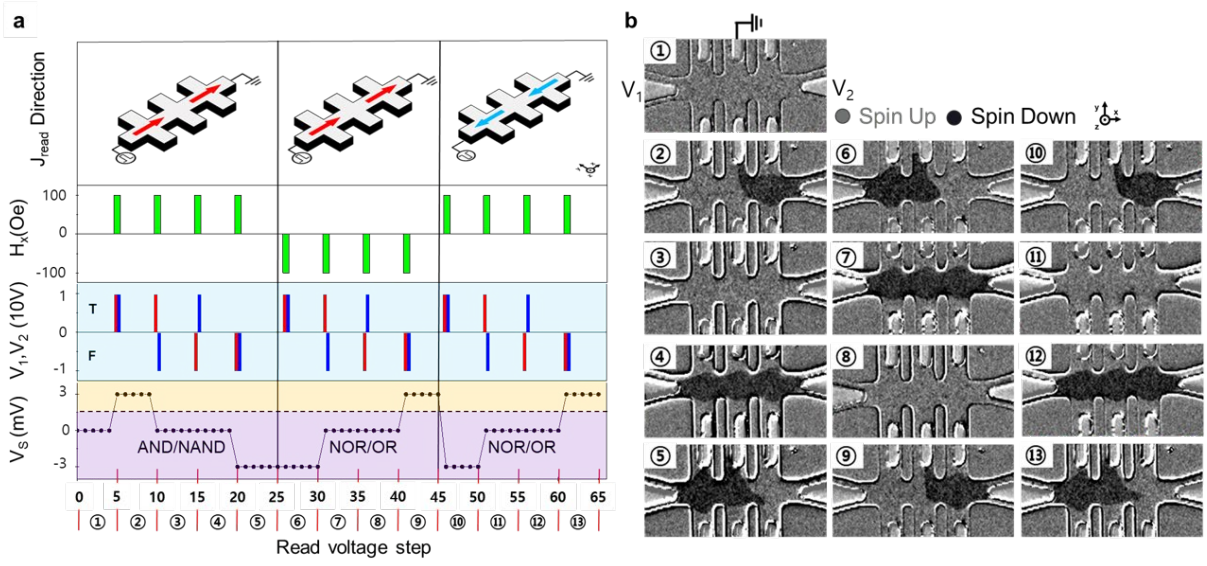

Fig. 2. (a) Logic gate output for the same series of write input parameters at ±V_1 and ± V_2 = ±10 V. V_1 and V_2. (b) Sequential MOKE images exhibiting the magnetic domains in each channel injecting inputs.

VI. POSSIBLE FUTRE PLANS FOR THE NEXT PROJECT

1) Approach I: Generation ofskrymion from magnetic strip pattern and their nature.

In future project, the ground is mainly to bring the generation/position determination of skyrmion from magnetic domain wall dynamics and magnetic strip patterns by manipulating diverse strip pattern widths, along with attaining a understanding of their skyrmion generation mechanism. In particular, we are planning to create an anti-ferromagnetically coupled magnetic skyrmion pairs (AFC-SkPs) from anti-ferrmagnetically coupled triple layers, which are expected to be unaffected by the skyrmion hall effect due to the coupled motion of two magnetic skyrmion pairs with opposite topological charges. The key scientific aspects of single and AFC-SkP dynamics are to exploit the following classes: (i) determination of various physical parameters in asymmetric multilayer hetero-structures which determine creation, annihilation, size and speed of single or AFC-S by means of PMA interface engineering treatments, together with attaining their physical nature observed from the magnetic strip patterns and (ii) scientific identification of creation/displacement of single and AFC-SkP driven by electrical current pulses.

2) Approach II: Fabrication of fully stacked MTJ junctions for efficient detection.

The second objective of future project aims to promote the creation of outstanding values for the emulation of neuromorphic computing neuron and synapse functions by identifying novel but practical AFC-SkPs dynamics, along with facilitating an anti-ferromagnetic exchange coupling (AFC) in FM/non-magnetic metal/FM frames serving as a single spin channel layer. Thus, this work requires design and manufacturing a basic AFC-SkP- driven neuron/synapse units by implementing fabrication process technologies (iv) evaluation of a basic integrate-and-fire functions of neuron and variation in

conductance (connection strength) of synapse unit. Among crucial prerequisites for the realization of AFC-SkP-driven neuromorphic neuron and synapse units, monitoring current-induced AFC-SkPs by means of purely electrical means is highly necessary. Thus, one approach for supporting academic bases for implementation of Al device is to detect transverse Hall resistivity in patterned multilayer systems. However, it is expected that the difference in the Hall resistance induced by AFC-SkPs is extremely small (~nΩ). Thus, the second objective of this project is to develop the fully stacked MTJ junctions for the electrical detection of AFC-SkP due to the expected large difference in tunneling magnetoresistance (TMR), even though the fabrication is really complicated in the university level: that is, manufacturing and evaluation of a basic single and AFC-SkP- driven neuron/synapse units will be conducted by implementing fabrication process technologies.

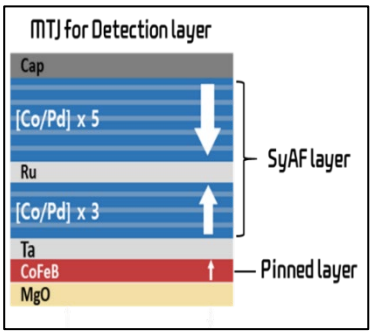

VII. PARTICIPANTS

Jin Pyo Hong: Department of Physics, Hanyang University (HYU), Seoul 04763, Republic of Korea
Jeong hun Shin: Department of Physics, Hanyang University (HYU), Seoul 04763, Republic of Korea
Jeon Woo Seo: Department of Physics, Hanyang University (HYU), Seoul 04763, Republic of Korea
Da Seul Hyeon, Department of Physics, Hanyang University (HYU), Seoul 04763, Republic of Korea

VII. PRODUCTS (PUBLICATIONS)

Not published yet